Research Article | Vol. 27, No. 15 / 22 July 2019 / Optics Express 21306
Optics EXPRESS

Octave-spanning single-cycle middle-infrared generation through optical parametric amplification in $LiGaS_2$

BO-HAN CHEN,[1,2] EMANUEL WITTMANN,[3] YUYA MORIMOTO,[1,2] PETER BAUM,[1,2,4,5] AND EBERHARD RIEDLE[3,6]

[1]Ludwig-Maximilians-Universität München, Am Coulombwall 1, 85748 Garching, Germany
[2]Max-Planck-Institute of Quantum Optics, Hans-Kopfermann-Str. 1, 85748 Garching, Germany
[3]LS für BioMolekulare Optik, Ludwig-Maximilians-Universität München, Oettingenstr. 67, 80538 München, Germany
[4]Universität Konstanz, Universitätsstraße 10, 78464 Konstanz, Germany
[5]peter.baum@uni-konstanz.de
[6]eberhard.riedle@physik.uni-muenchen.de

Abstract: We report the generation of extremely broadband and inherently phase-locked mid-infrared pulses covering the 5 to 11 µm region. The concept is based on two stages of optical parametric amplification starting from a 270-fs Yb:KGW laser source. A continuum seeded, second harmonic pumped pre-amplifier in β-BaB_2O_4 (BBO) produces tailored broadband near-infrared pulses that are subsequently mixed with the fundamental pump pulses in $LiGaS_2$ (LGS) for mid-infrared generation and amplification. The pulse bandwidth and chirp is managed entirely by selected optical filters and bulk material. We find an overall quantum efficiency of 1% and a mid-infrared spectrum smoothly covering 5-11 µm with a pulse energy of 220 nJ at 50 kHz repetition rate. Electro-optic sampling with 12-fs long white-light pulses directly from self-compression in a YAG crystal reveals near-single-cycle mid-infrared pulses (32 fs) with passively stable carrier-envelope phase. Such pulses will be ideal for producing attosecond electron pulses or for advancing molecular fingerprint spectroscopy.

1. Introduction

Few-cycle, high-field and phase-stable laser pulses in the mid-infrared (MIR) range of the optical spectrum are essential for many applications [1–3], especially for strong-field physics in solids [4], all-optical electron pulse compression [5] or molecular fingerprint spectroscopy [6–9]. Direct broadband laser sources are rare in the MIR due to lack of suitable materials. Researchers are therefore invoking nonlinear optical conversions, for example difference frequency generation or optical rectification in nonlinear crystals [10–13] such as GaSe or $AgGaS_2$ [14,15], filaments [16,17] or plasmas [18]. A quite new material is $LiGaS_2$ (LGS) [19–24] which offers a broadband transparency range (0.32–11.6 µm) and a large bandgap of ~4 eV that leads to very weak two-photon absorption for Ti:sapphire-based (~800 nm) or Yb-based (~1030 nm) laser pulses. LGS consequently combines a sufficiently large $\chi^{(2)}$ with a comparatively high optical damage threshold, especially at high repetition rates. The proper comparison of the various crystals requires simultaneous consideration of the amplification bandwidth, i.e. the useable crystal thickness, and the effective nonlinearity. This is where LGS performs best.

Historically, the relevant $\chi^{(2)}$ processes are classified as difference frequency generation (DFG), optical parametric amplification (OPA) and optical rectification (OR). In DFG, two waves with a difference of the carrier frequency equal to the desired MIR frequency are overlapped in a suitable nonlinear crystal to generate the MIR. It is often assumed that the photon number of

#363816 https://doi.org/10.1364/OE.27.021306
Journal © 2019 Received 8 Apr 2019; revised 14 Jun 2019; accepted 14 Jun 2019; published 16 Jul 2019

Optics EXPRESS

the weaker of the two beams limits the conversion. However, an intense short wavelength pump combined with a weak longer wavelength seed (signal) can lead to a much higher number of difference frequency (idler) photons as signal photons supplied. This is then the regime of OPA: the signal simultaneously gets amplified. In OR, both generating waves are taken out of one common pump beam if the bandwidth of this pulse is broader than the desired MIR frequency.

There are a number of challenges when transferring these DFG/OPA and OR concepts to the MIR. A broad phase matching and a proper temporal overlap of all involved spectral components are needed for efficient conversion. The width and form of the generating spectra and the output spectrum have to be carefully controlled to match the transparency range of the crystal in order to avoid heating and destruction. Such damage was reported in LGS crystals in earlier work [25]. Last but not least one needs to avoid any other nonlinear effects that inherently occur at the high intensities, e.g., self- or cross-phase modulation and Kerr lensing.

In this work, we report an OPA concept for producing an octave-spanning MIR spectrum and near-single-cycle pulses with high peak power and locked carrier-envelope phase while avoiding all of the above-mentioned problems. The work builds on our earlier reports about a related concept to generate CEP stable few cycle pulses in the 2 to 5 µm range [8,26–28]. We combine a noncollinear OPA (NOPA) pumped by the second harmonic of a 1026 nm Yb:KGW-based pump laser with a collinear amplifier pumped by the residual fundamental pulses. The amplified seed pulse minimizes the pump intensity and power needed for the final MIR generation and provides the necessary tailored spectrum needed for optimum efficiency and for avoiding damage. In this way damage of the LGS crystal is avoided. A rather thin crystal allows the use of a fairly small spot on the crystal that avoids issues with crystal inhomogeneity. The chirp is managed entirely with bulk materials and without the need for prism or grating sequences [29].

Our approach combines a set of straightforward and dedicated nonlinear optical frequency conversion stages for a stepwise and flexible control of power, phase, beam profile and stability. As compared to the currently popular spectral broadening of the full pump laser output in various media, we use just a small amount of light to obtain the necessary broadening and frequency shift in a bulk YAG crystal and subsequently add power by a first OPA stage. This concept allows to control and adjust the pulses' spectral and dispersive properties without the need for specially tailored chirped mirrors or luck with the properties of the nonlinear process. By performing the final MIR generation with two well-controlled and clean pulses, we avoid detrimental couplings between bandwidth, efficiency, fluctuations and spatial beam quality and can control the interplay between them for meeting the requirements of the following experiments. With only one more nonlinear conversion step as compared to spectral broadening and OR, the overall energy conversion efficiency is quite competitive.

2. Experimental setup

Figure 1 depicts the experiment that covers an area of less than 1 m^2. An Yb:KGW laser system (Pharos PH1-20, Light Conversion) delivers 270-fs pulses at a central wavelength of 1026 nm at a selected repetition rate of 50 kHz. A pulse energy of 187 µJ is used for the reported MIR experiments while the remaining ~200 µJ are driving a THz-based electron compressor [5,30] for other purposes in electron microscopy [31]. The 187 µJ are split into three arms: A first part of ~2 µJ (Fig. 1, red dotted line) is used to produce ultrashort probe pulses (yellow) for electro-optic sampling (EOS) of the MIR pulses.

The second part with 138 µJ (solid red line) goes into a noncollinear optical parametric amplifier system (NOPA, dotted outline) in which ~2 µJ are used for white-light generation [32]; 136 µJ are used for second-harmonic generation (green line) with 30% efficiency. 40 µJ at 513 nm are used to pump the NOPA crystal. A YAG crystal with a thickness of 10 mm is used to generate a broad plateau-like white-light on the near-infrared side of the fundamental. Thinner YAG plates did not provide sufficient broadening towards the NIR. Alternatively we successfully

Optics EXPRESS

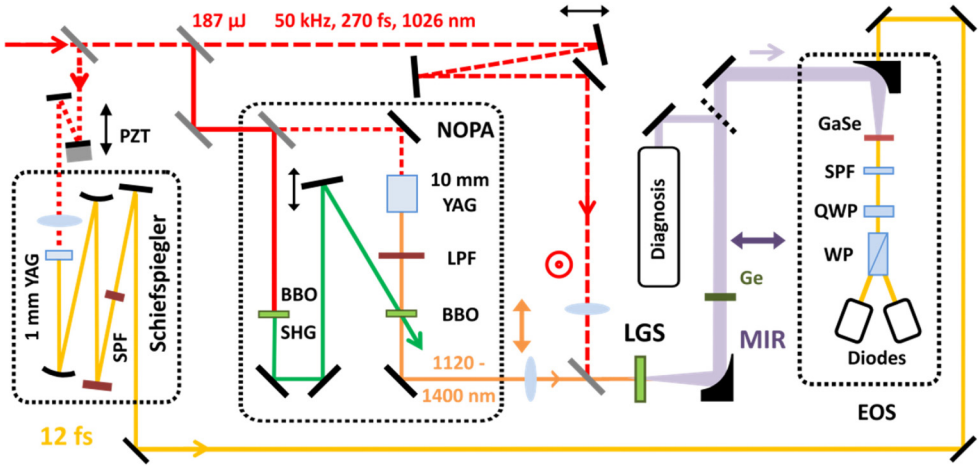

Fig. 1. Experimental setup. BBO, β-BaB_2O_4 crystal; LGS, $LiGaS_2$ crystal; YAG, $Y_3Al_5O_{12}$ crystal; Ge, Germanium plate with 4.5 µm LP filter coating; SHG, second-harmonic generation; LPF, longpass filter; SPF, shortpass filter; PZT, piezo electric transducer; EOS, electro-optic sampling; QWP, quarter-wave plate; WP, Wollaston prism. Note the absence of any pulse compression except by bulk material. The polarization of the three waves interacting in the LGS crystal is indicated.

tested an undoped Gadolinium Orthosilicate (GSO) crystal for the NIR continuum generation. It shows a very flat spectrum up to 1700nm.

The NIR side of the YAG white-light allows direct amplification of the broadband 1200 nm pulses needed for the MIR generation. This approach is found to be superior compared to seeding the amplifier collinearly at 900 nm and using the resulting idler at 1200 nm for the subsequent mixing/amplification. We do not use a collinear geometry because it would require non-trivial dichroic mirrors or filters for the separation of pump, signal and idler after amplification that would likely lead to temporal phase-distortions of the output pulse. The small noncollinearity slightly reduces the amplification bandwidth to a value still broad enough for the present purpose [33]. The NOPA crystal is a 3-mm thick Type I β-BaB_2O_4 crystal (BBO) at a cut angle of 24.5° and a noncollinearity angle of ~1-2°. The $1/e^2$ diameters of the seed beam and pump beam are both roughly 400 µm at the BBO. A longpass filter (High Performance longpass 1100 nm, Edmund Optics) blocks white-light wavelengths below 1120 nm in order to filter out the remaining fundamental light and to restrict the final MIR spectrum to below 12 µm where LGS would absorb. Figure 2(a) shows the pump laser spectrum (red) in comparison to the NOPA output spectrum (orange), ranging from 1120 nm to 1400 nm. The output pulse energy is 5 µJ. A concave spherical silver mirror (f = 500 mm) is used for beam collimation towards the next stage. The output of the NOPA subsystem are broadband, µJ-level pulses around 1200 nm to serve as seed light for the MIR generation.

In the subsequent amplification stage, 47 µJ pulses at 1026 nm are used to collinearly pump a LGS crystal. We use a type I orientation (xz cut) at a nominal cut angle of 47.9°. The various beam polarizations are shown in Fig. 1. A crystal thickness of 0.5 mm provides broadband phase matching and keeps the group velocity mismatch between pump and seed pulses sufficiently small (67 fs/mm). The phase matching is extremely broad already for a crystal orientation optimized for the central frequency and becomes even broader with a 0.5° additional tilt (see red and black solid lines in Fig. 2(b)). A 4 mm crystal [25] would render a much narrower spectrum (see black dotted line). The use of a 0.5 mm LGS crystal is possible due to the pre-amplification.

Optics EXPRESS

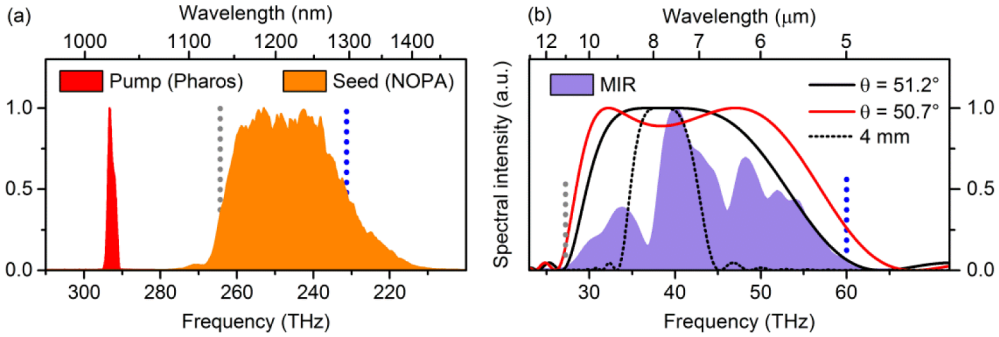

Fig. 2. Spectra of the three key pulses involved. (a) Narrow spectrum of the laser pulses (red) and broadband spectrum of the NOPA output (orange). The grey and blue dotted line corresponds to frequencies that are needed to generate 11 and 5 μm by DFG. (b) MIR spectrum after OPA in LGS. Phase matching term $\mathrm{sinc}^2(\Delta k$: phase mismatch, d: crystal thickness) for a 0.5 mm LGS crystal at perfect phase matching (black) and optimized for bandwidth (red). For comparison the sinc^2 curve for a 4 mm crystal is shown (black dotted).

This time we employ a collinear geometry in order to avoid angular dispersion in the MIR output. The broadband NOPA beam (Fig. 2(a), orange) and the narrowband fundamental beam (Fig. 2(a), red) are combined with a dichroic mirror that reflects 1100 - 1320 nm and transmits around 1026 nm. Imperfections of this beam combiner slightly reduce the pump and seed energy before the LGS crystal from 47 μJ and 5 μJ to 37 μJ and 4 μJ. This loss is tolerable in view of the above-mentioned benefits of collinear amplification.

The LGS crystal is placed considerably behind the focal planes to adjust the peak intensity to low enough values. This also helps to decrease the influence of the spherical aberration and compensates for small Kerr lensing effects. The $1/e^2$ beam diameters are ~700 μm for the pump beam and ~300 μm for the seed beam at the LGS crystal. The peak intensities are 70 GW/cm^2 and 65 GW/cm^2, respectively. These rather moderate intensities avoid the onset of self-focusing, spectral broadening, cross-polarized wave generation, and thermal lensing effects or crystal damage. The precise values of the spot size were optimized for MIR output power and bandwidth. For starting values, a desired gain of 3 was used in a plane wave approximation to estimate the needed intensity and thereby the spot size of the pump beam to start with.

After the LGS crystal, a longpass filter coated onto a 1-mm thick Germanium substrate (4.50 μm longpass OD > 3.0, Edmund Optics Inc.) filters out the remaining pump and seed beams. Neither of the pulses is intense enough to induce any nonlinear dynamics. We obtain the MIR spectrum shown in Fig. 2(b), measured with a Fourier-transform spectrometer (L-FTS, LASNIX). The spectrum spans the expected wavelength range of 5 - 11 μm with a rather smooth envelope and supports a Fourier limited pulse duration of 30.3 fs (FWHM). Note that the spectrum is shown on a linear scale, contrary to other reports where the spectral power density is shown on a logarithmic scale [17,19]. The direction of the energy scale in Fig. 2(a) is chosen opposite to the one in Fig. 2(b) to highlight that in the OPA process the higher-frequency seed photons are linked to the lower-frequency MIR photons. Matching positions are marked by the dotted grey and blue lines, showing the intended correspondence. The dips in the spectrum are attributed to interferences inside the spectrometer, residual reflectivity modulations in the optics and the absorption of air around 6.0 and 6.6 μm. Also the dip in the phase matching efficiency might contribute; see Fig. 2(b).

The MIR output power after the longpass Ge filter is 11 mW at a repetition rate of 50 kHz, corresponding to a pulse energy of 220 nJ. The quantum efficiency of the LGS stage, defined as the number of generated MIR photons divided by the number of input seed photons, is 31%.

Optics EXPRESS

Other optimizations of the setup with a 1-mm thick LGS crystal provided more than two times higher output pulse energies at the cost of some spectral bandwidth.

3. Pulse compression and characterization

3.1. Dispersion estimation

A central challenge in broadband MIR generation is dispersion management and compression, because chirped mirrors at wavelengths > 5 µm are still inefficient [34]. Alternatives like prism or grating sequences introduce additional higher order phase and are lossy and complicated to align in the MIR. Our setup therefore relies exclusively on bulk material for chirp management and pulse compression. In the collinear LGS amplifier it is necessary to match the two pulse durations to similar values in order to make best use of all the photons [35]. Fortunately, the near-infrared NOPA always produces (at sufficient amplification bandwidth) output pulses that are only slightly shorter than the pump pulse length, independently of the white-light chirp. Without any special effort, we therefore mix in the LGS crystal 170-fs long seed pulses (chirped) with 270-fs long pump pulses from the laser (near Fourier-limited).

In order to implement the envisioned all-bulk compression, we first consider theoretically all group delay contributions and their transfer during the nonlinear processes. The NIR NOPA output builds on the chirp of the white-light caused by the dispersion of YAG. More positive chirp is added by the longpass filter on a 3 mm fused silica substrate, the 3 mm BBO crystal and the focusing optics. The 1120-1400 nm output spectrum further acquires some positive chirp from roughly 90% of the 0.5 mm LGS crystal. Considering most of the mixing crystal for the NIR dispersion reflects the fact that the main MIR output is generated at the very end of the crystal (see below). The MIR generation process converts this positive chirp into negatively chirped pulses in the MIR due to difference frequency mixing of the pump and the seed pulse. Some further negative chirp is obtained from roughly the last 10% of the LGS crystal which has negative group delay dispersion in the MIR. The major part of the MIR is indeed generated in the final part of the crystal as with any OPA out of saturation. A small thickness of normally dispersive material in transmission, e.g., Germanium, should therefore be suitable for pulse compression.

Figure 3 reports a calculation based on the dispersion curves of all materials, including the air, and shows the estimated group delay (GD) of the pulses at different stages. We see a rather flat group delay dispersion with only a minor degree of higher orders. The result suggests that simply a few mm of Ge material should be suitable for optimal pulse compression. Varying the amount of Ge through tilting of the plate allows to fine tune the compression.

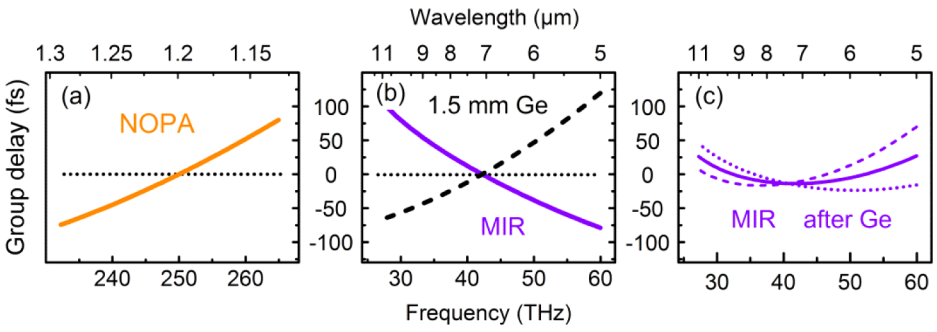

Fig. 3. Calculated group delay curves of the pulses at the different stages. (a) NOPA seed at 90% of the LGS crystal. (b) MIR pulses directly after generation (purple), in comparison to the group delay of 1.5 mm of Ge (black, dashed). (c) MIR pulses after passing through 1.0 (dotted), 1.5 (solid) and 2.0 mm (dashed) of Ge.

Optics EXPRESS

The data in Fig. 3(a) reproduces well the measured 170-fs length of the NOPA output. The fact that the NIR seed pulse does not get chirped much in the propagation is due to the fact that the wavelength is quite close to the zero dispersion point of fused silica and the other optical materials. Beyond the reported calculation we expect some additional GD contributions from the various dielectric filters.

3.2. Electro-optic sampling (EOS)

In order to characterize the MIR pulses in the temporal domain, we employ electro-optic sampling [36]. Short probe pulses are obtained from self-compression during continuum generation in a 1-mm YAG crystal. The effective focus inside the YAG is set to produce a single-filament only in the last few µm before the exit surface, in order to minimize dispersion and terminate the filament before group velocity dispersion effects become significant [32,37].

A Schiefspiegler arrangement (tilted-component telescope) [37] is applied for all-reflective and nonastigmatic beam refocusing of these ultrashort continuum pulses. The R = -150 mm concave mirror is placed 127 mm from the YAG plate. The angle of incidence at this mirror is 3.4°. The subsequent convex mirror with R = +200 mm is placed at 103 mm distance and at an angle of incidence of 8.9°. The resulting focus is located about 0.5 m after the second mirror and can be fine-tuned by the mirror distances while slightly tweaking the second angle of incidence. A shortpass filter (XIS0780, Asahi Spectra USA Inc.) used in reflection cuts out the chirped high frequency parts of the continuum. Another shortpass filter (High Performance shortpass 950 nm, Edmund Optics, 1 mm substrate thickness) is used to block the residual fundamental light at 1026 nm. Figure 4 shows the spectrum and an intensity autocorrelation measurement [38], revealing a 12-fs duration which is sufficient for EOS of the MIR pulses.

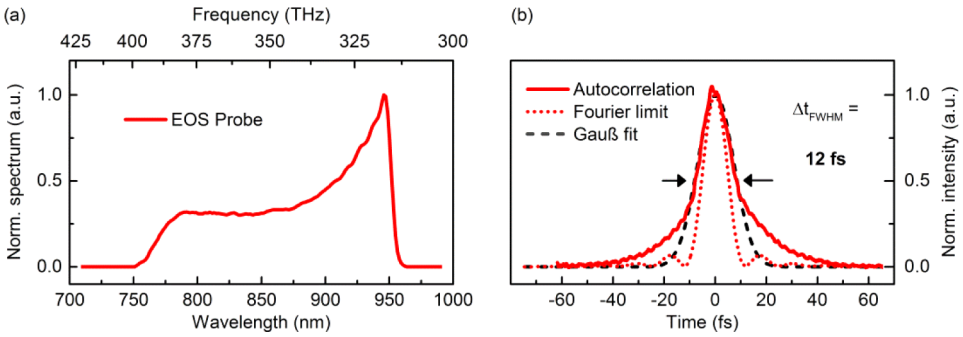

Fig. 4. Short, weak probe pulses for EOS, obtained directly from white-light generation. (a) Spectrum measured after 2 shortpass filters. (b) Intensity autocorrelation measurement of the probe pulses (red); red dotted curve, Fourier-limited pulse shape of the spectrum shown in Fig. 4(a); black dashed curve, Gauß fit to the autocorrelation trace.

The sampling element is a free-standing 20-µm thick GaSe crystal (Eksma) oriented for sum-frequency mixing between the MIR pulses and the white-light probe. A shortpass filter (High Performance shortpass 850 nm, Edmund Optics) removes the non-interacting spectral components in order to reduce the detection noise [39]. A quarter-wave plate and a Wollaston prism guide the two different polarizations onto two matched photodetectors of our own design [40], slightly modified to account for the higher repetition rate of 50 kHz. The shot-noise limit for detection is $2.6 \cdot 10^{-5}$ for a quantum efficiency of 80% of the detector, assuming 0.5 nJ gate pule energy. The signals of the detectors are digitized continuously with a PicoScope 5000 Series oscilloscope (model 5444A, Pico Technology Ltd.) at 14 bit resolution and with a sampling interval of 100 ns. Typically scan durations are 1 s, amounting to $1 \cdot 10^7$ samples per trace.

Optics EXPRESS

Figure 5(a) shows the EOS data for the case of 2 mm of bulk Ge for pulse compression. The blue curve shows the measured raw EOS signal. It is slightly limited on the short-wavelength side (<5 µm) by the finite duration of the probe pulse (12 fs) and on the long-wavelength side (>10.5 µm) by the EOS crystal thickness and its limited phase-matching bandwidth. By considering the measured probe pulse profile (see Fig. 4(b)) and the phase matching of GaSe, we obtain the spectral response function of our EOS measurement [41]. The final MIR field (Fig. 5(a) as the red curve) is then obtained by Fourier transformation, spectral correction and back-transformation. We see an ultrashort pulse of 32 fs duration (FWHM) at ~7.5 µm center wavelength with 1.4 optical cycles in the main lobe. 93% of the energy is contained in the main pulse. The central peak has a 1.3 times stronger electric and magnetic field than the second-strongest field cycle at –23 fs. This ratio would increase to 1.9 in the case of zero carrier-envelope phase. Assuming a focus size with a diameter of two wavelengths, a peak electric field strength of 3 GV/m and a peak magnetic field of 10 T could be achieved.

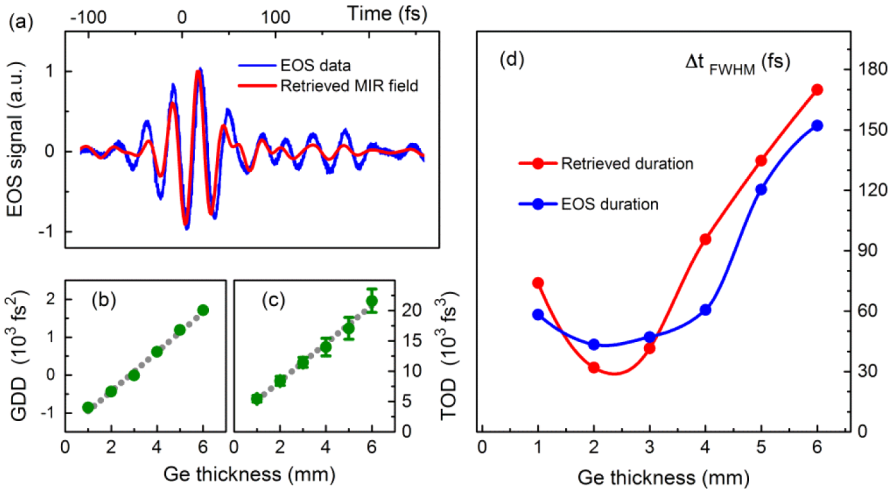

Fig. 5. Electric field of the MIR pulses and systematic study of pulse compression. (a) EOS data (blue) and retrieved electric field (red). (b) GD dispersion added by Ge. (c) Third order dispersion added. (d) MIR pulse duration as a function of Ge thickness.

Figures 5(b) and 5(c) show a more systematic study of the applied bulk compression concept. The measured group delay dispersion (GDD) and third order dispersion (TOD) of the MIR pulse are plotted as a function of the amount of Ge in the beam path. Linear fits (dashed) reveal ~520 fs^2/mm and ~3130 fs^3/mm, respectively. Figure 5(d) shows the measured pulse duration (FWHM) from EOS as a function of the Ge thickness. We see that the shortest pulses are achieved with about 2 mm of additional Ge.

A decisive advantage of our compression concept is that Fourier-limited MIR pulses can be obtained without any chirped mirrors or other special dispersive elements in the MIR. The measured pulse duration of 32 fs compares very well to the Fourier limit of 30.3 fs, showing that not only the linear chirp but also the higher orders are well compensated, as intended (see Fig. 3). In contrast to OR approaches, our inter-pulse MIR generation allows to apply available chirped mirrors for the NIR range (NOPA output) to control the MIR output even further. No direct MIR phase control is needed.

4. Beam quality

The spatial beam quality of the MIR output is crucial for many applications, especially in electron-pulse compression [30]. Figure 6(a) shows the MIR beam profile measured by a

Optics EXPRESS

broadband pyroelectric array camera (Pyrocam IIIHR, Spiricon, Ophir Photonics). Figure 6(b) shows the vertical and horizontal beam caustics, revealing M^2 values of 1.8 and 1.7, respectively. The slight astigmatism comes probably from residual misalignments of the focusing parabola. For the broadband pulses it is decisive to know whether all spectral components propagate collinearly or the beam suffers from angular dispersion or pulse front tilt. No detrimental tilt is expected in our concept because the first noncollinear stage amplifies the seed beam and idler generation is collinear in the second stage. Figure 6(c) shows four spectra taken in the far field of the beam at the four positions indicated by 1-4 in Fig. 6(a). We see sufficient homogeneity and no indication of spatial chirp.

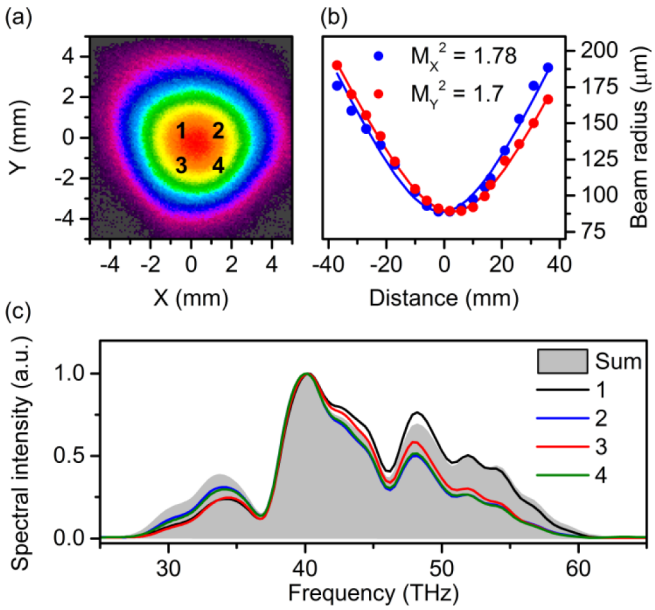

Fig. 6. Beam quality measurement. (a) MIR beam profile. (b) Beam caustics in the vertical (red, y) and horizontal axis (blue, x). (c) Spectra measured at different position in the MIR beam as indicated in (a) in comparison to the total spectrum (grey).

5. Power scalability and stability, CEP stability

In order to demonstrate that we indeed achieve genuine parametric amplification of the MIR pulses and not only see difference frequency radiation, we report in Fig. 7 several experiments on power dependencies. Figure 7(a) illustrates the quantities involved. Figure 7(b) shows the measured scaling of the MIR output energy when changing the amount of applied 1120-1400 nm light. We see an almost linear scaling, with only a slight onset of saturation. More seed energy would only partially be beneficial for the present pump energy and beam geometries.

Figure 7(c) shows the output pulse energy as a function of the 1026 nm pump pulse energy. Here we observe approximately a $\sinh^2$ dependence as expected from the coupled wave equations for optical parametric amplification. Further scaling of the amplification efficiency seems possible by increasing the pump power. Our concept is therefore not limited to the reported values and can be scaled up if more fundamental laser light is available.

Figure 7(d) shows the gain factor of our 1120-1400 nm amplification. Plotted is the output seed energy (right axis) as a function of the pump pulse energy and the corresponding gain (left axis), defined as the output seed energy divided by the output seed energy with no pump. The measured values are substantially larger than one and therefore show that we are in the regime

Optics EXPRESS

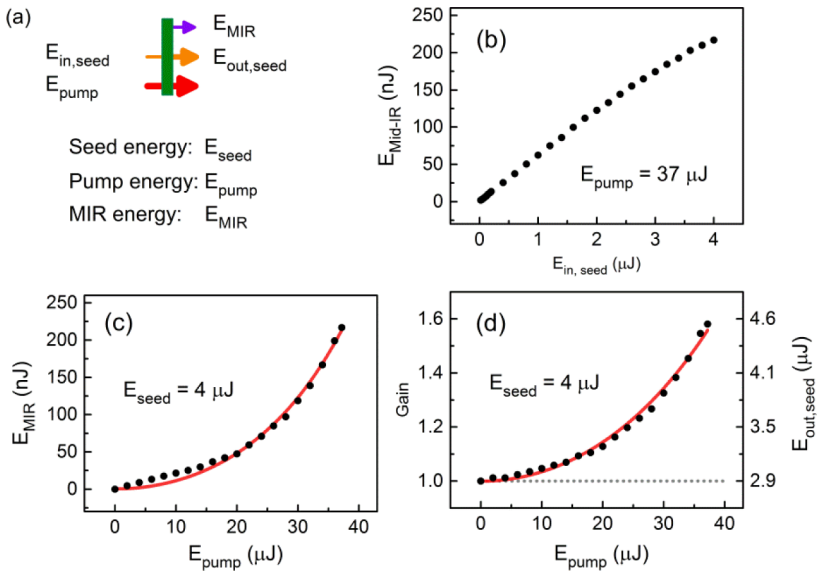

Fig. 7. Energy dependence of the amplification in LGS. (a) The three interacting beams. (b) Output MIR energy at fixed pump energy as a function of seed energy. (c) Output MIR at fixed seed as a function of pump energy. Red line shows the $\sinh^2$ fit. (d) Gain measurement at fixed seed and increasing pump energy. Red line shows the $\cosh^2$ fit.

where MIR radiation is generated and simultaneously amplified in the LGS crystal. This justifies the assumption made above, that the switch from NIR NOPA output light to MIR wavelengths effectively happens close to the end of the LGS crystal. While varying the pump or the seed energy, we never observed any significant changes of the spectrum or bandwidth of the MIR output. This result means that we have no secondary or cascaded nonlinear optical processes besides the intended optical parametric amplification. Consequently, the MIR output is very stable.

Figure 8(a) shows a long-term scan of the MIR power, measured every second for more than 13 hours. The drifts (averaged over 60 s) amount to less than 0.47% rms. Figure 8(b) shows part of the data on shorter time scales (1 s averaging). The fluctuations amount to merely 0.39% rms. The pulse-to-pulse fluctuations are measured over 1000 shots with an amplified photodetector (MCT, Thorlabs) and amount to 0.63% rms. These values demonstrate the high stability of our approach on any time scale that could be relevant for applications.

The MIR output pulses have a stable carrier-envelope phase (CEP) because the seed pulses have the identical phase fluctuations $\Delta\varphi$ as the fundamental laser pulses in both amplification stages. Consequently, the idler of the second stage becomes passively phase-locked and the MIR pulses have a stable CEP. Figure 9(a) shows a repeated measurement of EOS traces every 7 seconds over one hour. Figure 9(b) shows the extracted CEP values, averaged over one minute each. A faster time scale is reported in Fig. 9(c). For both time ranges, the CEP fluctuations are less than 0.053π or 165 mrad. For single shot resolution of the CEP fluctuations, the EOS delay is set to the zero crossing with the strongest temporal gradient and the signal is recorded for each laser shot. The slope of the signal change is calibrated and the measurement then directly renders the CEP fluctuation. The result is shown in Fig. 9(d) for a 4-second scan, with every 800^{th} point displayed. The resulting rms value, taking into account all of the data, is 85 mrad. The results of a second scan over a window of 1 s are shown in Fig. 9(e), resulting in 93 mrad rms fluctuation.

Optics EXPRESS

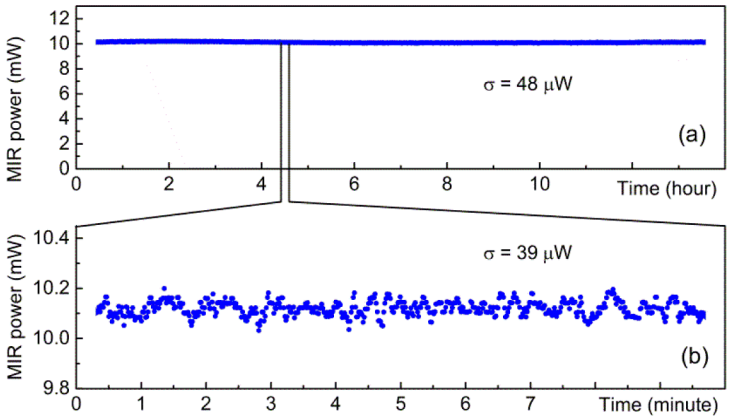

Fig. 8. Long-term power stability. (a) Mid-infrared power averaged over every minute. (b) Raw measurement with one data point taken every second.

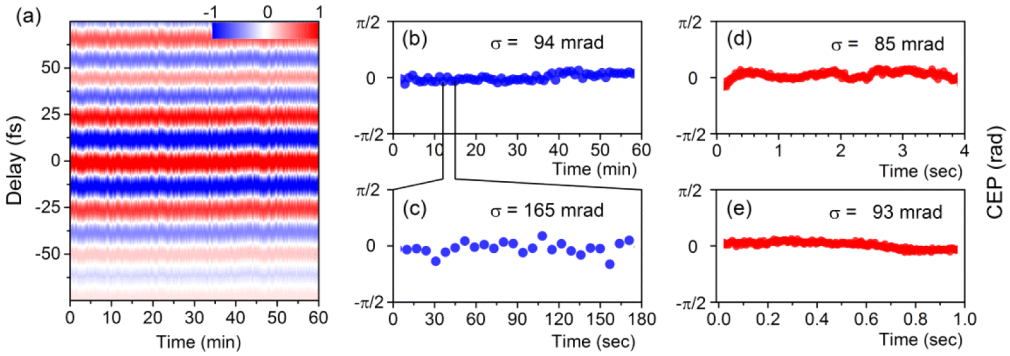

Fig. 9. Stability of the carrier-envelope phase (CEP). (a) EOS traces measured repetitively over one hour, with data points taken every 7 seconds. (b) Evaluated carrier-envelope phase values. (c) Carrier-envelope phase measured as rapidly as possible in complete electro-optic sampling scans (every 7 seconds). (d) Single-shot CEP stability over 4 seconds (200,000 pulses, every 800th shown). (e) Single-shot CEP stability over 1 sec (50,000 pulses, every 200th shown).

The whole measurement is performed without any active delay stabilization, neither between the two arms of the difference frequency generation nor for the electro-optic sampling. This result demonstrates the passive phase cancellation in our MIR generation and furthermore shows the value of the reported simplifications by a careful design of noncollinear and collinear arrangements, chirp management with bulk materials and application of intensities well below the onset of higher-order nonlinearities. It should be noted that the reported values are strictly speaking upper limits because the additional possible fluctuation of the gate pulses (white-light) and its beam path length are also contributing to the measurement.

6. Discussion and future aspects

For our intended use of the MIR pulses in femtosecond electron scattering, there remain only few points of further desire. An optimized beam combiner for pump and seed pulses could support an even broader seed spectrum and consequently we could produce even shorter pulses in the MIR, approaching the sub-cycle regime. The phase matching of LGS supports this. Alternatively GaSe could be used to produce pulses at even longer wavelengths.

Optics EXPRESS

At present, the SHG efficiency in the NOPA is 30%, a value that should not be increased significantly in order to avoid temporal and spatial deteriorations of the pulses and beam. The NOPA is running with a 29% quantum efficiency (513 to 1200 nm), again very close to the maximum that avoids back conversion and pulse deterioration. Finally, the MIR mixing works at an amplification of 1.6. This corresponds to a 60% conversion of the 1200 nm seed photons in a DFG picture, close to full conversion. Referenced to the 1026-nm pump, the quantum efficiency is already 5%. A higher output up to 30% could only be achieved with harder pumping at the risk of crystal damage. Unless some added power instabilities, beam deteriorations or CEP fluctuations would be acceptable, we therefore think that the reported system is close to the optimum for most applications.

Higher MIR power could readily be achieved by using one of the available fs pump lasers with tens or even hundreds Watt power. Figures 7(b) and 7(c) show that both an increased pump intensity and also increased seed levels will lead to more output. An appropriate balance between the respective intensities will avoid the amplification of vacuum fluctuations [42] and issues with crystal damage.

Using a longer LGS crystal, for example 1 mm, is another alternative to increase the output power if the bandwidth of the MIR pulses is not a primary concern. In principle, the system is tunable, by changing the delay and noncollinearity angle in the NOPA and by adjusting the phase-matching conditions at the LGS. Tunable MIR pulses are valuable for spectroscopy, for controlling materials [43] or for light wave synthesis from multiple sources [44]. All of these suggestions can easily be implemented with the presented inter-pulse mixing scheme and its ample possibilities to adjust a certain parameter without changing other ones.

In summary, the reported results show how broadband single-cycle MIR pulses can be generated with simple OPA concepts and all-bulk compression. The 32 fs output pulse length is a shortening of nearly an order of magnitude from the pump pulse length. Two systems related to the reported one are already successfully running in two other laboratories in collaborative efforts. Our own system will serve for attosecond electron microscopy and diffraction [45] of complex materials under strong-field, single-cycle excitation [46].

Funding

H2020 European Research Council (ERC) (647771); Munich-Centre for Advanced Photonics (MAP).

Acknowledgments

We thank Christina Hofer and Ioachim Pupeza for their loan of the 20-µm EOS crystal and acknowledge preliminary work together with Rupert Huber and Philipp Merkl.

References

1. R. A. Kaindl, M. Wurm, K. Reimann, P. Hamm, A. M. Weiner, and M. Woerner, "Generation, shaping, and characterization of intense femtosecond pulses tunable from 3 to 20 µm," J. Opt. Soc. Am. B **17**(12), 2086–2094 (2000).
2. H. Pires, M. Baudisch, D. Sanchez, M. Hemmer, and J. Biegert, "Ultrashort pulse generation in the mid-IR," Prog. Quantum Electron. **43**, 1–30 (2015).
3. V. Petrov, "Frequency down-conversion of solid-state laser sources to the mid-infrared spectral range using non-oxide nonlinear crystals," Prog. Quantum Electron. **42**, 1–106 (2015).
4. M. Hohenleutner, F. Langer, O. Schubert, M. Knorr, U. Huttner, S. W. Koch, M. Kira, and R. Huber, "Real-time observation of interfering crystal electrons in high-harmonic generation," Nature **523**(7562), 572–575 (2015).
5. C. Kealhofer, W. Schneider, D. Ehberger, A. Ryabov, F. Krausz, and P. Baum, "All-optical control and metrology of electron pulses," Science **352**(6284), 429–433 (2016).
6. F. Adler, M. J. Thorpe, K. C. Cossel, and J. Ye, "Cavity-enhanced direct frequency comb spectroscopy: Technology and applications," Annu. Rev. Anal. Chem. **3**(1), 175–205 (2010).
7. A. Schliesser, N. Picqué, and T. W. Hänsch, "Mid-infrared frequency combs," Nat. Photonics **6**(7), 440–449 (2012).

Optics EXPRESS

8. M. Bradler, J. C. Werhahn, D. Hutzler, S. Fuhrmann, R. Heider, E. Riedle, H. Iglev, and R. Kienberger, "A novel setup for femtosecond pump-repump-probe IR spectroscopy with few cycle CEP stable pulses," Opt. Express **21**(17), 20145–20158 (2013).
9. H. Timmers, A. Kowligy, A. Lind, F. C. Cruz, N. Nader, M. Silfies, G. Ycas, T. K. Allison, P. G. Schunemann, S. B. Papp, and S. A. Diddams, "Molecular fingerprinting with bright, broadband infrared frequency combs," Optica **5**(6), 727–732 (2018).
10. G. Andriukaitis, T. Balčiūnas, S. Ališauskas, A. Pugžlys, A. Baltuška, T. Popmintchev, M. C. Chen, M. M. Murnane, and H. C. Kapteyn, "90 GW peak power few-cycle mid-infrared pulses from an optical parametric amplifier," Opt. Lett. **36**(15), 2755–2757 (2011).
11. U. Elu, M. Baudisch, H. Pires, F. Tani, M. H. Frosz, F. Köttig, A. Ermolov, P. St.J. Russell, and J. Biegert, "High average power and single-cycle pulses from a mid-IR optical parametric chirped pulse amplifier," Optica **4**(9), 1024–1029 (2017).
12. O. Novák, P. R. Krogen, T. Kroh, T. Mocek, F. X. Kärtner, and K. H. Hong, "Femtosecond 8.5 μm source based on intrapulse difference-frequency generation of 2.1 μm pulses," Opt. Lett. **43**(6), 1335–1338 (2018).
13. S. Vasilyev, I. S. Moskalev, V. O. Smolski, J. M. Peppers, M. Mirov, A. V. Muraviev, K. Zawilski, P. G. Schunemann, S. B. Mirov, K. L. Vodopyanov, and V. P. Gapontsev, "Super-octave longwave mid-infrared coherent transients produced by optical rectification of few-cycle 2.5-μm pulses," Optica **6**(1), 111–114 (2019).
14. A. Sell, A. Leitenstorfer, and R. Huber, "Phase-locked generation and field-resolved detection of widely tunable terahertz pulses with amplitudes exceeding 100 MV/cm," Opt. Lett. **33**(23), 2767–2769 (2008).
15. K. Reimann, R. P. Smith, A. M. Weiner, T. Elsaesser, and M. Woerner, "Direct field-resolved detection of terahertz transients with amplitudes of megavolts per centimeter," Opt. Lett. **28**(6), 471–473 (2003).
16. Y. Nomura, H. Shirai, K. Ishii, N. Tsurumachi, A. A. Voronin, A. M. Zheltikov, and T. Fuji, "Phase-stable sub-cycle mid-infrared conical emission from filamentation in gases," Opt. Express **20**(22), 24741–24747 (2012).
17. A. V. Mitrofanov, A. A. Voronin, D. A. Sidorov-Biryukov, S. I. Mitryukovsky, A. B. Fedotov, E. E. Serebryannikov, D. V. Meshchankin, V. Shumakova, S. Ališauskas, A. Pugžlys, V. Y. Panchenko, A. Baltuška, and A. M. Zheltikov, "Subterawatt few-cycle mid-infrared pulses from a single filament," Optica **3**(3), 299–302 (2016).
18. Z. Nie, C. H. Pai, J. F. Hua, C. J. Zhang, Y. P. Wu, Y. Wan, F. Li, J. Zhang, Z. Cheng, Q. Q. Su, S. Liu, Y. Ma, X. N. Ning, Y. X. He, W. Lu, H. H. Chu, J. Wang, W. B. Mori, and C. Joshi, "Relativistic single-cycle tunable infrared pulses generated from a tailored plasma density structure," Nat. Photonics **12**(8), 489–494 (2018).
19. I. Pupeza, D. Sánchez, J. Zhang, N. Lilienfein, M. Seidel, N. Karpowicz, T. Paasch-Colberg, I. Znakovskaya, M. Pescher, W. Schweinberger, V. Pervak, E. Fill, O. Pronin, Z. Wei, F. Krausz, A. Apolonski, and J. Biegert, "High-power sub-two-cycle mid-infrared pulses at 100 MHz repetition rate," Nat. Photonics **9**(11), 721–724 (2015).
20. M. Knorr, J. Raab, M. Tauer, P. Merkl, D. Peller, E. Wittmann, E. Riedle, C. Lange, and R. Huber, "Phase-locked multi-terahertz electric fields exceeding 13 MV/cm at a 190 kHz repetition rate," Opt. Lett. **42**(21), 4367–4370 (2017).
21. K. Kato, K. Miyata, L. Isaenko, S. Lobanov, V. Vedenyapin, and V. Petrov, "Phase-matching properties of $LiGaS_2$ in the 1.025-10.910 μm spectral range," Opt. Lett. **42**(21), 4363–4366 (2017).
22. M. Huber, W. Schweinberger, F. Stutzki, J. Limpert, I. Pupeza, and O. Pronin, "Active intensity noise suppression for a broadband mid-infrared laser source," Opt. Express **25**(19), 22499–22509 (2017).
23. B. H. Chen, T. Nagy, and P. Baum, "Efficient middle-infrared generation in $LiGaS_2$ by simultaneous spectral broadening and difference-frequency generation," Opt. Lett. **43**(12), 2876 (2018).
24. M. Seidel, X. Xiao, S. A. Hussain, G. Arisholm, A. Hartung, K. T. Zawilski, P. G. Schunemann, F. Habel, M. Trubetskov, V. Pervak, O. Pronin, and F. Krausz, "Multi-watt, multi-octave, mid-infrared femtosecond source," Sci. Adv. **4**(4), eaaq1526 (2018).
25. S. B. Penwell, L. Whaley-Mayda, and A. Tokmakoff, "Single-stage MHz mid-IR OPA using $LiGaS_2$ and a fiber laser pump source," Opt. Lett. **43**(6), 1363–1366 (2018).
26. M. Bradler, C. Homann, and E. Riedle, "Mid-IR femtosecond pulse generation on the microjoule level up to 5μm at high repetition rates," Opt. Lett. **36**(21), 4212–4214 (2011).
27. C. Homann, M. Bradler, M. Förster, P. Hommelhoff, and E. Riedle, "Carrier-envelope phase stable sub-two-cycle pulses tunable around 1.8 μm at 100 kHz," Opt. Lett. **37**(10), 1673–1675 (2012).
28. M. Neuhaus, H. Fuest, M. Seeger, J. Schötz, M. Trubetskov, P. Russbueldt, H. D. Hoffmann, E. Riedle, Zs. Major, V. Pervak, M. F. Kling, and P. Wnuk, "10 W CEP-stable few-cycle source at 2 μm with 100 kHz repetition rate," Opt. Express **26**(13), 16074–16085 (2018).
29. P. Baum, S. Lochbrunner, and E. Riedle, "Generation of tunable 7-fs ultraviolet pulses: achromatic phase matching and chirp management," Appl. Phys. B: Lasers Opt. **79**(8), 1027–1032 (2004).
30. D. Ehberger, A. Ryabov, and P. Baum, "Tilted electron pulses," Phys. Rev. Lett. **121**(9), 094801 (2018).
31. A. Ryabov and P. Baum, "Electron microscopy of electromagnetic waveforms," Science **353**(6297), 374–377 (2016).
32. M. Bradler, P. Baum, and E. Riedle, "Femtosecond continuum generation in bulk laser host materials with sub-μJ pump pulses," Appl. Phys. B: Lasers Opt. **97**(3), 561–574 (2009).
33. J. Piel, M. Beutter, and E. Riedle, "20-50-fs pulses tunable across the near infrared from a blue-pumped noncollinear parametric amplifier," Opt. Lett. **25**(3), 180–182 (2000).
34. F. Habel and V. Pervak, "Dispersive mirror for the mid-infrared spectral range of 9-11.5 μm," Appl. Opt. **56**(4), C71–C74 (2017).

Optics EXPRESS

35. I. Z. Kozma, P. Baum, S. Lochbrunner, and E. Riedle, "Widely tunable sub-30 fs ultraviolet pulses by chirped sum frequency mixing," Opt. Express **11**(23), 3110–3115 (2003).
36. C. Kübler, R. Huber, S. Tübel, and A. Leitenstorfer, "Ultrabroadband detection of multi-terahertz field transients with GaSe electro-optic sensors: Approaching the near infrared," Appl. Phys. Lett. **85**(16), 3360–3362 (2004).
37. E. Wittmann, M. Bradler, and E. Riedle, "Direct generation of 7 fs whitelight pulses from bulk sapphire," in *Preceedings of the 19th International Conference on Ultrafast Phenomena* 162, 725–728 (2014).
38. I. Z. Kozma, P. Baum, U. Schmidhammer, S. Lochbrunner, and E. Riedle, "Compact autocorrelator for the online measurement of tunable 10 femtosecond pulses," Rev. Sci. Instrum. **75**(7), 2323–2327 (2004).
39. M. Porer, J. Ménard, and R. Huber, "Shot noise reduced terahertz detection via spectrally postfiltered electro-optic sampling," Opt. Lett. **39**(8), 2435–2438 (2014).
40. C. Schriever, S. Lochbrunner, E. Riedle, and D. J. Nesbitt, "Ultrasensitive ultraviolet-visible 20 fs absorption spectroscopy of low vapor pressure molecules in the gas phase," Rev. Sci. Instrum. **79**(1), 013107 (2008).
41. M. Knorr, P. Steinleitner, J. Raab, I. Gronwald, P. Merkl, C. Lange, and R. Huber, "Ultrabroadband etalon-free detection of infrared transients by van-der-Waals contacted sub-10-μ m GaSe detectors," Opt. Express **26**(15), 19059–19066 (2018).
42. C. Homann and E. Riedle, "Direct measurement of the effective input noise power of an optical parametric amplifier," Laser Photonics Rev. **7**(4), 580–588 (2013).
43. A. von Hoegen, R. Mankowsky, M. Fechner, M. Först, and A. Cavalleri, "Probing the interatomic potential of solids with strong-field nonlinear phononics," Nature **555**(7694), 79–82 (2018).
44. H. K. Liang, P. Krogen, Z. Wang, H. Park, T. Kroh, K. Zawilski, P. Schunemann, J. Moses, L. F. DiMauro, F. X. Kärtner, and K. H. Hong, "High-energy mid-infrared sub-cycle pulse synthesis from a parametric amplifier," Nat. Commun. **8**(1), 141 (2017).
45. Y. Morimoto and P. Baum, "Diffraction and microscopy with attosecond electron pulse trains," Nat. Phys. **14**(3), 252–256 (2018).
46. V. S. Yakovlev, M. I. Stockman, F. Krausz, and P. Baum, "Atomic-scale diffractive imaging of sub-cycle electron dynamics in condensed matter," Sci. Rep. **5**(1), 14581 (2015).